Phosphate and polyphosphate anion recognition by a dinuclear copper(II) complex of an unsymmetrical squaramide[i]

Catarina V. Esteves[a], Judite Costa[b], David Esteban-Gómez[c], Pedro Lamosa[a], Hélène Bernard[d], Carlos Platas-Iglesias[c], Raphäel Tripier[d] and Rita Delgado[a*]

[a] Instituto de Tecnologia Química e Biológica António Xavier, Universidade Nova de Lisboa, Av. da República, 2780-157 Oeiras, Portugal

[b] Research Institute for Medicines (iMed.ULisboa), Faculty of Pharmacy, Universidade de Lisboa, Av. Prof. Gama Pinto, 1649-003 Lisboa, Portugal

[c] Centro de Investigacións Científicas Avanzadas (CICA) and Departamento de Química, Universidade da Coruña, Campus da Zapateira-Rúa da Fraga 10, 15008 A Coruña, Spain

[d] Université de Brest, UMR-CNRS 6521, IBSAM, UFR des Sciences et Techniques, 6 Avenue Victor le Gorgeu, 29238 Brest Cedex 3, France

Dalton Transactions, volume 48, issue 27, pages 10104–10115, 21 July 2019
Submitted 4 April 2019, accepted 28 May 2019, first published 29 May 2019

How to cite:

C. V. Esteves, J. Costa, D. Esteban-Gómez, P. Lamosa, H. Bernard, C. Platas-Iglesias, R. Tripier and R. Delgado, Phosphate and polyphosphate anion recognition by a dinuclear copper(II) complex of an unsymmetrical squaramide, *Dalt. Trans.*, 2019, **48**, 10104–10115. DOI: 10.1039/C9DT01434A.

Abstract

In the search for receptors suitable for the recognition of phosphate or polyphosphate anions, a new unsymmetrical squaramide-based ligand bearing dipicolylamine (dpa) and ethylpiperazine units (**L**) was designed and prepared. The acid–base reactions of **L**, its copper(II) complexation behaviour and the binding of phosphate and polyphosphate anions by the copper(II) complexes used as receptors were evaluated. ^{1}H and ^{13}C NMR titrations of **L** performed in D_2O allowed the determination of its protonation sequence. The ligand **L** is able to coordinate two copper(II) cations forming thermodynamically stable dinuclear complexes likely having two water molecules bound to each metal centre, as supported by DFT calculations. Coordinated water molecules can be replaced by the O-donors of the phosphate/polyphosphate anions. The potentiometric studies showed that at 2 : 1 Cu^{2+} : **L** ratio the dinuclear $[Cu_2\mathbf{L}H_{-1}]^{3+}$ species predominates from pH ∼ 5 to ∼7, and hydroxodinuclear species prevail at pH > 7. ^{1}H NMR experiments in both H_2O/D_2O 9 : 1 v/v and in DMSO proved that copper(II) coordination provokes deprotonation of the squaramide NH bound to the ethylpiperazine moiety, resulting in $[Cu_2\mathbf{L}H_{-1}]^{3+}$ species. The dicopper(II) complexes of **L**, $[Cu_2\mathbf{L}H_{-i}]^{4-i}$, were used as the receptor for the uptake of some phosphate and polyphosphate anions. The receptor presents very high association constants with $HPPi^{3-}$ and ATP^{4-} and the determined K_{eff} showed that at physiological pH ATP^{4-} is selectively taken from an aqueous solution containing phenylphosphate ($PhPO_4^{2-}$), aminoethylphosphate ($Haep^{-}$), AMP^{2-} and ADP^{3-}, but $HPPi^{3-}$ strongly interferes. DFT calculations suggest that the strong interaction with $HPPi^{3-}$ and ATP^{4-} is related to the simultaneous coordination of the polyphosphate unit to the two copper(II) centres.

* delgado@itqb.unl.pt

Introduction

Anion recognition chemistry is nowadays a major research subject as anions are ubiquitous in nature and have enormous biological and environmental relevance. Anions play a sustaining role in the biological and ecological systems and the imbalance of their concentrations may lead to several diseases and ecological hazards. Therefore, the design of chemical architectures capable of specific anion recognition and its selective uptake from the medium is an important goal.[1] Since the report of a series of squaramide-based compounds as effective receptors for the recognition of carboxylate anions *via* squaramidic NH···O hydrogen bonding by A. Costa *et al.*,[2] many other related synthetic compounds and their binding studies with anions have been published.[3] The four-membered ring structure of squaramides, known for their rigidity and hydrogen bonding ability, has enabled the synthesis of many compounds for a number of applications, such as the already mentioned molecular recognition, but also in pharmaceuticals, bioconjugates, materials, organometallics, and organocatalysis.[4] However, to the best of our knowledge only one study was reported so far that used a squaramide-based compound as a ligand for copper(ii) complexation,[5] able to chromogenically sense this metal ion through formation of a zwitterion radical. A cryptand bearing a dimethyl cyclen and two squaramide moieties and its copper(ii) complex was studied by Micheloni *et al.*,[6] but the results proved that the metal cation is only bound by the cyclen moiety far away from both squaramide units, which only play a role in stabilizing F^- or Cl^- anions through the formation of hydrogen bonds.

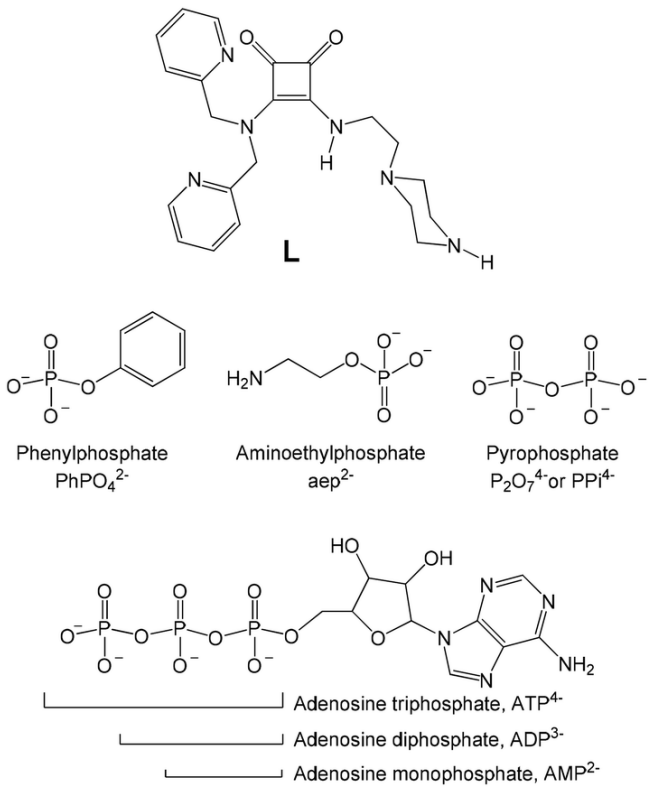

Scheme 1. The ligand prepared in this work and the studied phosphate and polyphosphate anions.

In the present study, the synthesis of a new unsymmetrical squaramide-based ligand bearing dipicolylamine (dpa) and ethylpiperazine units (**L**, Scheme 1) was undertaken. We hypothesized that the squaramide spacer should allow the formation of dinuclear copper(ii) complexes, in which the two metal centres are close enough to allow the simultaneous coordination of polyphosphate anions to both metal centres. Furthermore,

the ability of the squaramide unit to act as a hydrogen-bonding acceptor could reinforce the interaction with anions like ADP^{3-} and ATP^{4-}, which contain hydroxyl groups. Thus, the acid–base reactions of **L**, its copper(ii) complexation behaviour and the ability of the copper(ii) complexes to act as receptors for anions such as $PhPO_4^{2-}$, $Haep^{-}$, AMP^{2-}, ADP^{3-}, ATP^{4-}, and $HPPi^{3-}$ (Scheme 1) were investigated. Potentiometric and different spectroscopic techniques such as NMR and UV-vis studies were used, which were supported by DFT calculations.

Results and discussion

Synthesis

The **L** compound was prepared using a procedure involving two steps (see Scheme 2 and the Experimental section). In the first step, 2,2′-dipicolylamine (dpa) was added to 3,4-diethoxy-3-cyclobutene-1,2-dione (diethyl squarate). The reaction mixture was left standing for one week to promote the total reaction. It is known that the reduced nucleophilicity of aromatic secondary amines[4a] may lead to the formation of 1,3-squaraine together with the 1,2-squaramide,[7] and that the substitution orientation depends on both the amine nucleophilicity and the acidity of the medium.[8] Indeed, in the first step a squaraine was obtained as a side product, which was glued to the round bottom flask, but after decantation of the solvent the monosubstituted squaramate (**smdpa**) was obtained as crystals suitable for X-ray diffraction. The second step consisted of reacting **smdpa** with 2-(piperazin-1-yl)ethan-1-amine in 1 : 1 stoichiometry to yield almost quantitatively the unsymmetrically disubstituted squaramide (**L**).

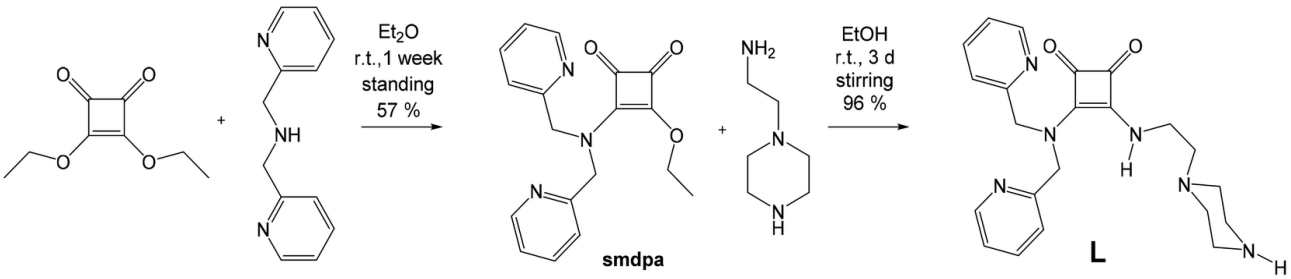

Scheme 2. Synthetic procedure to prepare **L**.

Single crystal X-ray diffraction study

The X-ray crystal structure of **smdpa**, shown in Fig. S1, evidences the coplanarity of the squaramidic N1 in relation to the squarate center. The lengths of the C2–O2 and C3–O3 bonds (1.223 and 1.220 Å, respectively) are slightly shorter than the ones observed on a similar aliphatic squaramate.[9] In contrast, the distances found for the C4–N1 and C1–O1 bonds of 1.319 and 1.332 Å, respectively, are longer. Moreover, both pyridine groups of the dpa moiety point to opposite directions, and the four C–C distances found for the squarate group are all different (C1–C2, 1.452 Å; C2–C3, 1.512 Å; C3–C4, 1.488 Å and C4–C1, 1.400 Å), as observed in other squaramates.[5]

Solution studies

Acid–base behaviour of L – potentiometric studies. The protonation constants of **L** were obtained from potentiometric titrations performed in aqueous solution at 298.2 K and in 0.10 M KNO_3. The results are collected in Table 1 and the speciation diagram of **L** is shown in Fig. 1. **L** instead of Hsdp designs the ligand

for simplicity reasons. In fact the amidic proton is too basic to be possible to determine its protonation constant under the conditions used here, but it is easily deprotonated by coordination to copper(ii), see below.

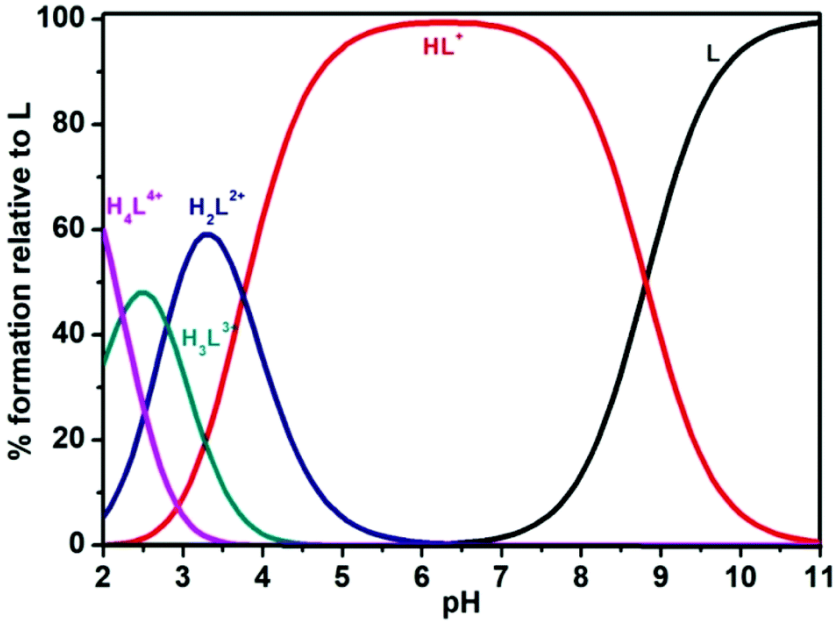

Fig. 1. Species distribution diagram of the **L** at $C_L = 1.0 \times 10^{-3}$ M.

Table 1. Overall (β_i^H, and β_i^D) and stepwise (K_i^H and K_i^D) protonation constants of **L** in H_2O and in D_2O solutions at 298.2 ± 0.1 K.

Equilibrium reaction[a]	Potentiometry[b] log β_i^H		^{1}H NMR titration[c] log β_i^D
L + H^+ ⇄ $H\mathbf{L}^+$	8.81(1)		9.75(1)
L + $2H^+$ ⇄ $H_2\mathbf{L}2^+$	12.57(2)		13.56(1)
L + $3H^+$ ⇄ $H_3\mathbf{L}^{3+}$	15.37(2)		16.30(1)
L + $4H^+$ ⇄ $H_4\mathbf{L}^{4+}$	17.61(9)		18.87(1)
	log K_i^H	log K_i^D	log K_i^H
L + H^+ ⇄ $H\mathbf{L}^+$	8.81(1)	9.75(1)	9.03,[c] 9.11[d]
$H\mathbf{L}^+$ + H^+ ⇄ $H_2\mathbf{L}^{2+}$	3.76(1)	3.81(1)	3.34,[c] 3.59[d]
$H_2\mathbf{L}^{2+}$ + H^+ ⇄ $H_3\mathbf{L}^{3+}$	2.80(2)	2.74(1)	2.32,[c] 2.59[d]
$H_3\mathbf{L}^{3+}$ + H^+ ⇄ $H_4\mathbf{L}^{4+}$	2.24(9)	2.57(1)	2.16,[c] 2.44[d]

[a] Values in parenthesis are standard deviations in the last significant figures. [b] I = 0.1 ± 0.01 M in KNO_3. [c] Values calculated from K^D_i using the equation of ref. 12. [d] Values calculated from K^D_i using the equation of ref. 13.

The first calculated protonation constant of 8.81 in log units is consistent with the protonation of the secondary amine of the piperazine ring (N^1H), and the remaining three constants of 3.76, 2.80 and 2.24 in log units must correspond to the protonation of the other centre of the piperazine arm (N^2) and to the two pyridine groups of dpa (N^4 and N^5). Under similar experimental conditions, *N*-ethylpiperazine presents two protonation constants of 9.20 and 4.76,[10] while for dpa the value of 7.11 is ascribed to the protonation of the secondary amine and the two very low constants of 2.48 and <2 for the protonation of the pyridine groups, as they are close to the already protonated amine (all values in log units).[11] However, based only on potentiometric measurements it is not possible to establish the protonation sequence; for such elucidation, it was necessary to perform ^{1}H and ^{13}C NMR titrations of the compound in D_2O (see below).

^{1}H and ^{13}C NMR studies. As mentioned above, in order to establish the protonation sequence of **L**, ^{1}H and ^{13}C NMR titrations were performed in D_2O at 298.2 K, as shown in Fig. 2 and Fig. S2 in the ESI.† To assign all resonances, the chemical shifts, peak integrations and multiplicity resulting from ^{1}H, ^{13}C NMR spectra and cross-peaks from NOESY, HMBC and HSQC experiments were taken into account.

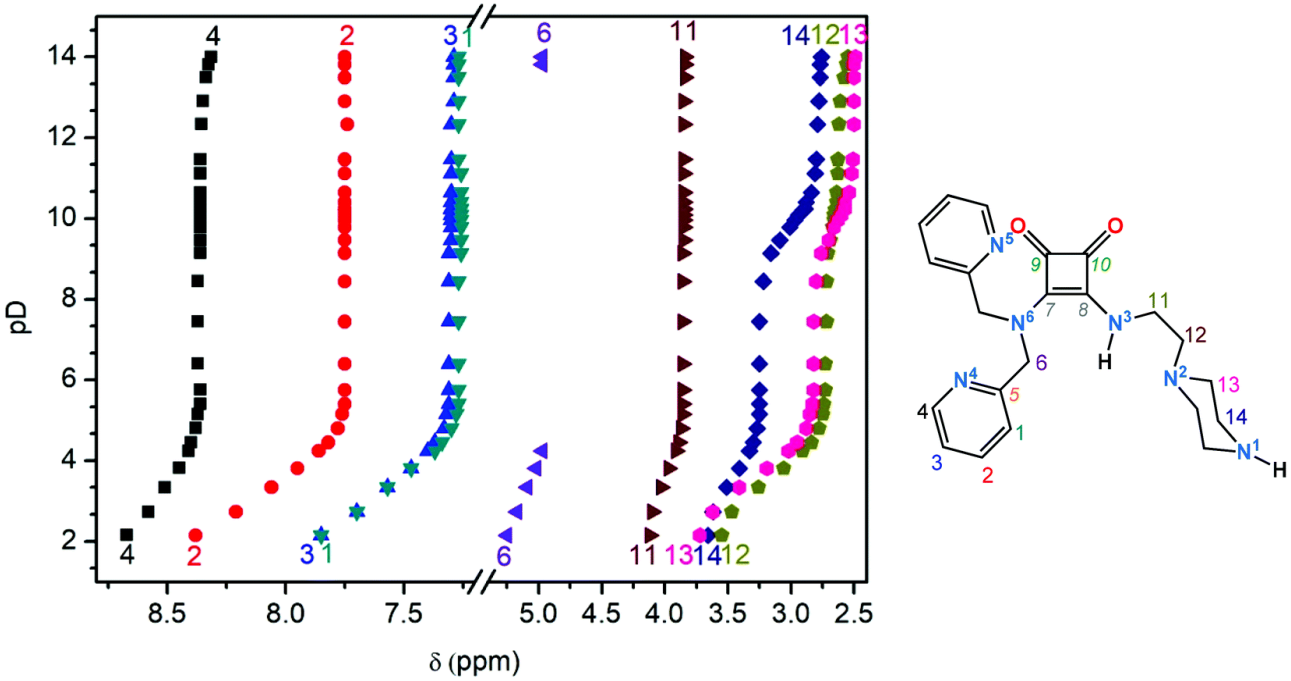

Fig. 2. ^{1}H NMR experimental chemical shifts (δ, ppm) as a function of pD observed during the titration of **L** with DCl or NaOD in D_2O at 298.2 K (left); structure of the compound with numbering of atoms (right).

The downfield region of the ^{1}H NMR spectrum presents four different signals at high pD corresponding to the H1–H4 protons from the dpa moiety. The signal due to H6 protons is observed close to the residual water peak (close to the region where a break has been inserted in Fig. 2). The upfield region displays also four signals that were assigned to the H11–H14 protons of the ethylpiperazine moiety. At the same pD the ^{13}C NMR spectrum presents nine signals in the downfield region, four of them corresponding to the C nuclei of the squaramide unit (C7–C10), and five to the dpa moiety (C1–C5). Five additional signals were observed in the upfield region, which correspond to the signal due to the CH_2 in the dpa moiety (C6), and the C atoms from the ethylpiperazine arm (C11–C14).

At high pD values (≥13.5) addition of NaOD to **L** causes slight shifts of H4, H6, H12 and H13 proton resonances, which is likely related to the breaking of hydrogen bonds. However, lowering the pD of

the **L** solution by addition of DCl causes significant changes in the chemical shifts of ^{1}H NMR resonances. The first changes were observed in the pD range of 11.46–7.44. In this region, the signal due to H14 protons strongly shifts downfield, while the signal of H13 protons suffered a moderate shift and the H1–H4 proton resonances from dpa maintained their chemical shifts. This unambiguously indicates that the first protonation occurred at the amine atom N^1. In the same pD region the signals of C13 and C14 experience marked upfield shifts, while that of C12 suffers a slight upfield shift and that of C11 does not significantly move.

As the addition of DCl progressed, the second inflexion occurred in the pD range of 5.75–2.15, where all the proton resonances initiated another downfield shift. The carbon resonances of C12, C6, C14 and C11 suffered important upfield shifts, which points out that the protonation of N^2 started to occur. Then as the pD continued to be lowered the protonation of N^4 and N^5 takes place, so that all the proton resonances continued their downfield movements. In the last two points recorded at low pD the resonances of H11 and H14 do not shift anymore, while the resonances of protons H1–H4 continue their downfield shifting, providing further evidence that the protonations of N^4 and N^5 are taking place. The carbon resonances of C1, C2, and C4–C6 broadened and almost collapsed to the baseline, an effect that should be related to the two protonation events taking place at the dpa moiety, which likely increases the rigidity of the molecule by the formation of intramolecular hydrogen-bonding interactions.

The protonation constants of **L** in D_2O (K^D_i) were also determined from the refinement of all the resonances of the ^{1}H NMR titration. The values are collected in Table 1, and converted to K^H_i in H_2O to be compared to those determined by potentiometry by using $pK^D_i = 0.32 + 1.044pK^H_i$,[12] and $pK^H_i = 0.42 + 0.929pK^{H*}_i$,[13] where pK^{H*}_i are the protonation constants determined by using pH* readings of D_2O solutions but electrodes calibrated in H_2O. The corresponding pK^H_i values, see also Table 1, show that the first equation led to closer values for the first and last constants although the second one affords closer values for the remaining constants, when compared to the more accurate constants obtained by potentiometry.[12]

Searching for the NH resonances in the ^{1}H NMR spectrum of **L** dissolved in $CDCl_3$, the signal at 8.30 ppm was found as a proton in a NH group and confirmed as bound to N^3 by ^{1}H–^{15}N HSQC experiments (Fig. S3 of the ESI†). Another resonance that did not produce any signal on the ^{1}H–^{13}C HSQC spectra was found at 1.73 ppm (Fig. S3 and S4 of the ESI†), but while N^3–H integrated to one, this resonance integrated to around four (bottom spectrum of Fig. S3 of the ESI†). Addition of water to the sample until a maximum of 3 μL resulted in increased intensity of this resonance, and when a big excess of water (30 μL) was added, the water molecules probably solvated the compound and the resonance integrates only to one unit, while the excess of water starts to appear around 5 ppm (top spectrum of Fig. S3 of the ESI†). This suggests that with a small amount of water the H_2O molecules are in fast exchange with the NH proton. Increasing the amount of water results in a shift of the water signal, so the system is in slow exchange due to a larger chemical shift difference between NH and H_2O protons. This might constitute a piece of evidence for the ability of this compound to receive water molecules probably through hydrogen bonding formation.

Copper(II) complexation behaviour of L

The ability of **L** to form complexes with copper(II) was evaluated in aqueous solution by the thermodynamic stability constants determined under the conditions described for the protonation studies. The values are collected in Table 2.

At a 2 : 1 Cu^{2+}/L ratio and below pH ~ 5 a fair amount of free copper(II) is observed as well as two mononuclear species $[CuH\mathbf{L}]^{3+}$ and $[Cu\mathbf{L}]^{2+}$ (see the species distribution diagram in Fig. 3), and an increasing amount of the dinuclear $[Cu_2\mathbf{L}H_{-1}]^{3+}$ species, which will be dominant between pH ~ 5 and ~7. At pH > 7 the hydroxodinuclear species prevail. The coordination of the second copper(II) cation needs to involve the deprotonation of the squaramidic NH, as confirmed by ^{1}H NMR experiments in DMSO (Fig. 5) and by DFT calculations, see below. Additionally, the stability constant values reported for piperazine and

piperazine-1,4-diylbis(methylene)bis(phosphonic acid) are very low (log K = 3.32 [14] and 3.18,[15] respectively). This fact is explained by the rigidity associated with the piperazine ring due to its chair conformation, which often results in non-coordination to the metal centre of one of the piperazine nitrogen atoms.[16] Due to this weak coordination of piperazine, it is reasonable to assume that the mononuclear $[Cu\mathbf{L}]^{2+}$ species involves the coordination of the dpa moiety. Coordination of the second copper(II) cation to **L** can induce the complete removal of the squaramidic proton NH linked to the ethylpiperazine unit, yielding the $[Cu_2\mathbf{L}H_{-1}]^{3+}$ species dominating from pH ~ 5 to 7. Then the removal of the second and subsequent protons is attributed to the deprotonation of H_2O molecules directly bound to one of the Cu centres.

Table 2. Overall ($\beta_{Cum}H_h\mathbf{L}$) and stepwise ($K_{Cum}H_h\mathbf{L}$) stability constants of the complexes of **L** with copper(II) at 298.2 ± 0.1 K and I = 0.10 ± 0.01 M KNO_3 in aqueous solution.

Equilibrium reaction[a]	log $\beta_{Cu_mH_hL}$
$Cu^{2+} + H^+ + \mathbf{L} \rightleftarrows [CuH\mathbf{L}]^{3+}$	13.96(9)
$Cu^{2+} + \mathbf{L} \rightleftarrows [Cu\mathbf{L}]^{2+}$	11.02(6)
$2Cu^{2+} + \mathbf{L} \rightleftarrows [Cu_2\mathbf{L}H_{-1}]^{3+} + H^+$	9.18(7)
$2Cu^{2+} + \mathbf{L} \rightleftarrows [Cu_2\mathbf{L}H_{-2}]^{2+} + 2H^+$	2.32(6)
$2Cu^{2+} + \mathbf{L} \rightleftarrows [Cu_2\mathbf{L}H_{-3}]^{+} + 3H^+$	−5.03(7)
$2Cu^{2+} + \mathbf{L} \rightleftarrows [Cu_2\mathbf{L}H_{-4}] + 4H^+$	−14.86(9)
	log $K_{Cu_mH_hL}$
$Cu^{2+} + H\mathbf{L}^+ \rightleftarrows [CuH\mathbf{L}]^{3+}$	2.94(8)
$Cu^{2+} + \mathbf{L} \rightleftarrows [Cu\mathbf{L}]^{2+}$	11.02(6)
$[Cu_2\mathbf{L}]^{4+} \rightleftarrows [Cu_2\mathbf{L}H_{-1}]^{3+} + H^+$	9.18(7)
$[Cu_2\mathbf{L}H_{-1}]^{3+} \rightleftarrows [Cu_2\mathbf{L}H_{-2}]^{2+} + H^+$	6.86(7)
$[Cu_2\mathbf{L}H_{-2}]^{2+} \rightleftarrows [Cu_2\mathbf{L}H_{-3}]^{+} + H^+$	7.35(7)
$[Cu_2\mathbf{L}H_{-3}]^{+} \rightleftarrows [Cu_2\mathbf{L}H_{-4}] + H^+$	9.83(8)

[a] Values in parenthesis are standard deviations in the last significant figures.

To gain structural insights into the copper(II) coordination sequence by the dpa or the ethylpiperazine units, respectively, ^{1}H NMR spectra were recorded upon addition of increasing amounts of copper(II) into H_2O/D_2O 9 : 1 v/v, at pH 7.4 and at 298.2 K (Fig. S6 of the ESI). When 0.25 equiv. of copper(II) were added to **L** both aromatic and aliphatic resonances shift slightly and lose resolution. Upon addition of 0.75 equiv. of copper(II) the resonances from the dpa moiety collapsed to the baseline, while the resonances from the ethylpiperazine unit only started to fell down to the baseline in the presence of 1.5 equiv. of copper(II). This indicates that the mononuclear copper(II) complex results from the coordination of the dpa moiety to the metal ion. Subsequently, the formation of the dinuclear complex involves the coordination of the ethylpiperazine unit to the metal ion.

To further investigate the effective proton removal of the squaramidic nitrogen by coordination of the second copper(II) center, experiments were conducted in organic solvents such as $CDCl_3$ (Fig. S5 of the ESI) and DMSO-d_6 (Fig. S6 of the ESI) in order to observe the N^3H resonance. In $CDCl_3$, it was only possible to prepare a solution with 0.5 : 1 Cu^{2+}/L ratio, as samples with a larger amount of copper(II) precipitate. Then, DMSO-d_6 was used. The ^{1}H NMR spectrum of the ligand recorded in the latter solvent shows the signal of

the N^3H resonance at 7.89 ppm. Overall, the region 7.25–8.75 ppm displays five signals integrating for nine protons (H1, H2, H3, H4 and N^3H). When up to one equivalent of copper(II) was added, the 7.25–8.75 region maintains a 9 : 2 intensity ratio with respect to the signals of H4 protons, as would be expected. Increasing the Cu^{2+}/L ratio beyond 1 : 1 decreases the relative intensity of the 7 to 7.76 ppm region, which can be attributed to the deprotonation of the squaramidic N^3H group.

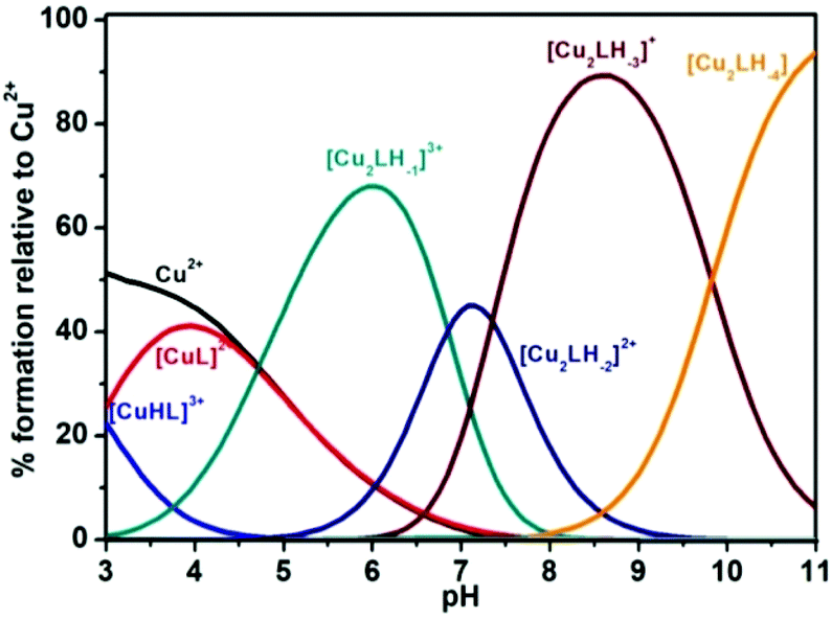

Fig. 3. Species distribution diagram obtained for the copper(II) complexes of **L** at 2 : 1 Cu^{2+}/**L** stoichiometry. $C_{Cu} = 2C_L = 2.0 \times 10^{-3}$ M.

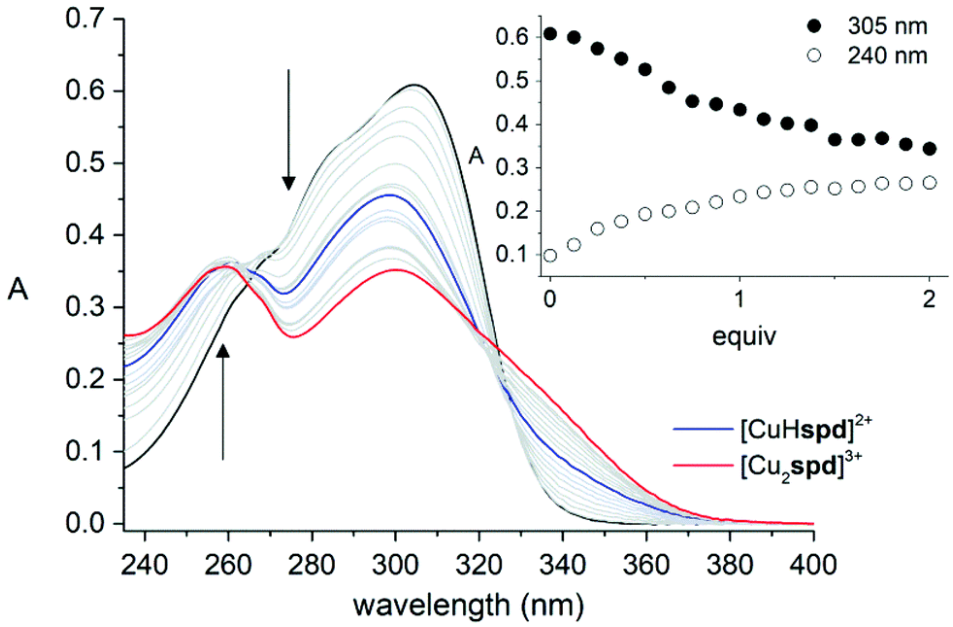

Fig. 4. UV-vis batch titration of **L** (2.89×10^{-5} M) with $Cu(NO_3)_2$ in buffered aqueous solution ([MOPS] = 2.5×10^{-2} M, pH = 7.4 and 298.2 K). The inset shows the spectral variations at the two selected wavelengths. Arrows show shoulders discussed in the text.

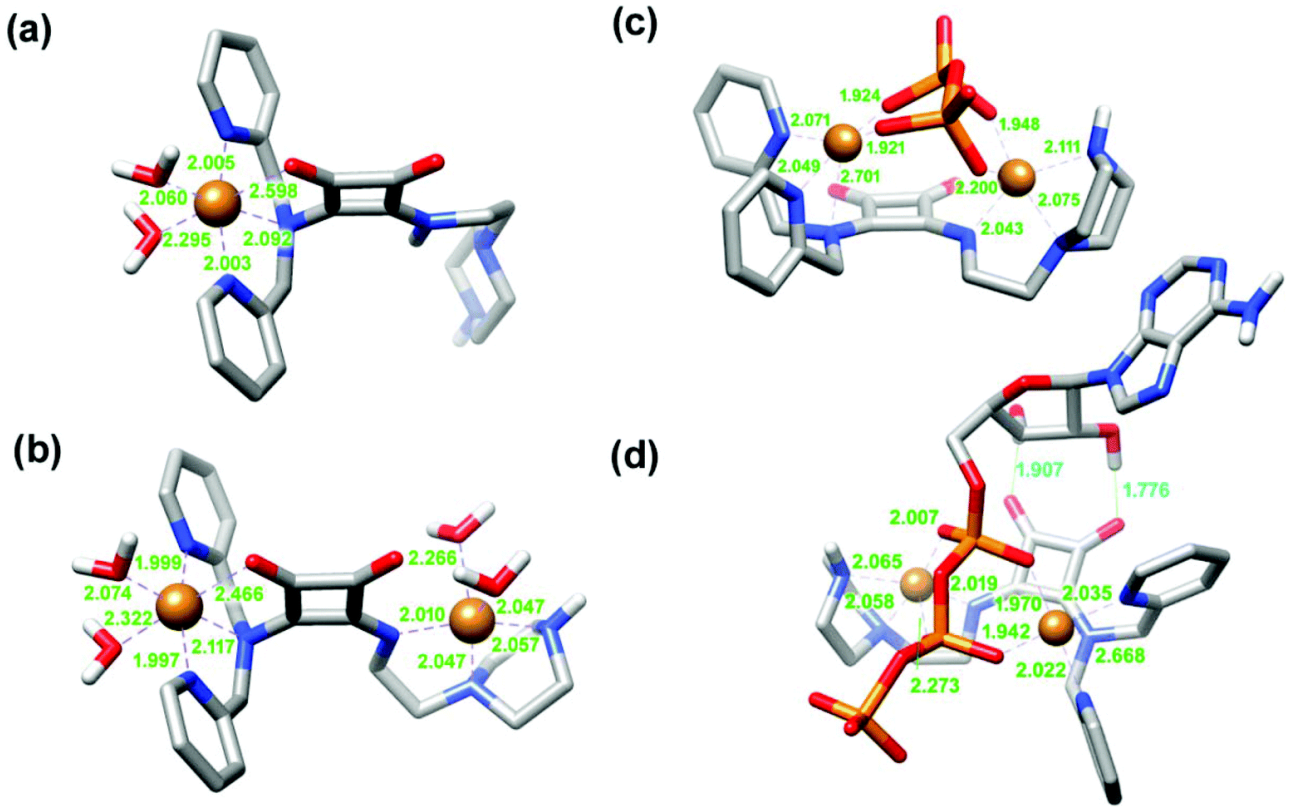

Fig. 5. Structures of the $[CuL]^{2+}$ (a), $[Cu_2LH_{-1}]^{3+}$ (b), $[Cu_2LH_{-1}(PPi)]^{-}$ (c) and $[Cu_2LH_{-1}(ATP)]^{-}$ (d) complexes obtained with DFT calculations. The numbers indicate the calculated distances in Å.

The UV-vis titration of the **L** ligand with copper(II) was also carried out in order to obtain information on the binding mode of the complex (Fig. 4 and Fig. S7 of the ESI). Addition of copper(II) to the ligand in aqueous solution buffered at pH 7.4 with MOPS (3-(*N*-morpholino)propanesulfonic acid), at 298.2 K, results in the development of a new weak absorption band in the visible region of the spectrum characteristic of Cu(II) d–d transitions, see Fig. S7 of the ESI. Upon addition of 1 equiv. of metal ion, the d–d absorption is observed as a broad feature with υ_{max} at 705 nm (ε = 80 M^{-1} cm^{-1}). These spectral data are consistent with those of $[Cu(dpa)(ClO_4)_2]$ and other dpa derivatives, which present a Jahn–Teller distorted octahedral coordination.[17] Addition of copper(II) solution from 1 to 2 equiv. causes a slight red shift of the absorption band, suggesting that the second metal ion presents either a Jahn–Teller distorted octahedral or square-planar geometry.

The absorption spectrum of **L** in the UV region (Fig. 4) is dominated by a rather intense absorption at 304 nm (ε = 21 000 M^{-1} cm^{-1}) with a characteristic shoulder at 280 nm ascribed to the squaramide unit.[18] A second shoulder on the high energy side at 260 nm is attributed to the absorption of the pyridyl rings of the ligand.[19] Addition of Cu(II) up to 1 equiv. causes a slight shift of the absorption maximum as its intensity decreases, with the simultaneous formation of two isosbestic points at 266 and 327 nm. Simultaneously, the shoulder at 260 nm becomes more defined as its intensity increases. These spectral changes are consistent with the coordination of both the pyridyl and squaramide units to the Cu(II) ion in the mononuclear $[CuL]^{2+}$ complex. Addition of Cu(II) from one to two equiv. causes additional changes in the absorption band at 300 nm, which decreases in intensity as a shoulder develops in the low energy side. At the same time, two isosbestic points at 264 and 319 nm are formed. In contrast, faint spectral variations are observed around 260 nm, where the absorption profile is dominated by the absorption of the pyridyl units. Thus, these data are consistent with the coordination (and subsequent deprotonation) of the squaramide unit to the second Cu(II) ion in the dinuclear $[Cu_2LH_{-1}]^{3+}$ species, in nice agreement with the NMR data described above.

DFT calculations were carried out to gain further insight into the structure of the $[CuL]^{2+}$ and $[Cu_2LH_{-1}]^{3+}$ species (see computational details below). The $[CuL]^{2+}$ complex shows the metal ion coordinated by the dpa moiety through the three nitrogen atoms and an oxygen atom of the squaramide unit (Fig. 5a). Two water molecules had to be added to the model to complete the copper(II) coordination environment, which can be described as distorted octahedral. The oxygen atom of the squaramide unit provides a weak coordination to the metal ion (Cu–O = 2.589 Å). The calculated structure is very similar to those observed in the solid state for dpa derivatives containing an additional urea group.[20]

The second metal ion is directly coordinated to the two N atoms of the piperazine unit and the deprotonated squaramide N atom (Fig. 5b). A chelate coordination of piperazine fragments has been observed previously in different X-ray structures.[21] Up to two water molecules had to be added to the model to complete the metal coordination environment, which can be described as square pyramidal. According to our calculations the amide nitrogen atom provides the strongest interaction with the metal ion (Fig. 5).

Table 3. Stepwise ($K_{Cu2}H_hLA$) association constants of the copper(II) complexes of **L** with the anions under study at 298.2 ± 0.1 K and I = 0.10 ± 0.01 M KNO_3 in aqueous solution.

Equilibrium reaction[a]	log $K_{Cu_2H_hLA}$
$[Cu_2LH_{-1}]^{3+} + HPhP^{-} \rightleftarrows [Cu_2L(PhP)]^{2+}$	3.57(3)
$[Cu_2LH_{-1}]^{3+} + PhP^{2-} \rightleftarrows [Cu_2LH_{-1}(PhP)]^{+}$	3.51(3)
$[CuL]^{2+} + [CuHaep]^{+} \rightleftarrows [Cu_2HL(aep)]^{3+}$	6.09(2)
$[Cu_2LH_{-1}]^{3+} + H_2aep \rightleftarrows [Cu_2HL(aep)]^{3+}$	4.47(2)
$[Cu_2LH_{-1}]^{3+} + Haep^{-} \rightleftarrows [Cu_2L(aep)]^{2+}$	4.78(2)
$[Cu_2LH_{-2}]^{2+} + Haep^{-} \rightleftarrows [Cu_2LH_{-1}(aep)]^{+}$	4.00(2)
$[Cu_2LH_{-1}]^{3+} + H_2AMP \rightleftarrows [Cu_2HL(AMP)]^{3+}$	4.05(3)
$[Cu_2LH_{-1}]^{3+} + HAMP^{-} \rightleftarrows [Cu_2L(AMP)]^{2+}$	3.96(2)
$[Cu_2LH_{-1}]^{3+} + AMP^{2-} \rightleftarrows [Cu_2LH_{-1}(AMP)]^{+}$	4.25(2)
$[Cu_2LH_{-2}]^{2+} + AMP^{2-} \rightleftarrows [Cu_2LH_{-2}(AMP)]$	3.47(4)
$[Cu_2LH_{-1}]^{3+} + H_2ADP^{-} \rightleftarrows [Cu_2HL(ADP)]^{2+}$	4.43(7)
$[Cu_2LH_{-1}]^{3+} + HADP^{2-} \rightleftarrows [Cu_2L(ADP)]^{+}$	4.12(8)
$[Cu_2LH_{-1}]^{3+} + ADP^{3-} \rightleftarrows [Cu_2LH_{-1}(ADP)]$	5.46(3)
$[Cu_2LH_{-1}]^{3+} + H_2ATP^{2-} \rightleftarrows [Cu_2HL(ATP)]^{+}$	5.30(5)
$[Cu_2LH_{-1}]^{3+} + HATP^{3-} \rightleftarrows [Cu_2L(ATP)]$	5.80(3)
$[Cu_2LH_{-1}]^{3+} + ATP^{4-} \rightleftarrows [Cu_2LH_{-1}(ATP)]^{-}$	7.31(2)
$[Cu_2LH_{-2}]^{2+} + ATP^{4-} \rightleftarrows [Cu_2LH_{-2}(ATP)]^{2-}$	5.57(3)
$[CuHL]^{3+} + [CuHPPi] \rightleftarrows [Cu_2H_2L(PPi)]^{3+}$	4.60(4)
$[Cu_2LH_{-1}]^{3+} + H_2PPi^{2-} \rightleftarrows [Cu_2HL(PPi)]^{+}$	3.29(9)
$[Cu_2LH_{-1}]^{3+} + HPPi^{3-} \rightleftarrows [Cu_2L(PPi)]$	4.89(4)
$[Cu_2LH_{-2}]^{2+} + PPi^{4-} \rightleftarrows [Cu_2LH_{-2}(PPi)]^{3-}$	6.62(3)

[a] Values in parenthesis are standard deviations in the last significant figures; L denotes the ligand and A the anion in general.

Cascade species formed by the copper(II) complexes of L with phenylphosphate, aminoethylphosphate, and polyphosphate anions

The association constants of the copper(II) complexes of **L** with the anions (cascade species) were determined by potentiometry under the experimental conditions described above, and the results are collected in Table 3 for the stepwise constants and in Table S4 of the ESI for the overall constants. The required protonation constants of the anions and their stability constants with copper(II) (Tables S1 and S2 of the ESI and ref. 22) as well as the association constants of the anions directly bound to protonated forms of **L** were also determined under the same conditions (Table S3 of the ESI), although the values for ATP^{4-}, ADP^{3-}, AMP^{2-} and PhP^{2-} were too low to be determined.

Only 1 : 1 cascade species of the dicopper(II) complex of **L** and the studied anions were found, as shown in Table 3. Other receptor : anion ratios were considered, such as 1 : 2, which could not provide good adjustments to the experimental data.

The distribution species diagrams for the cascade species formed between the copper(II) complexes of **L** and the anions are shown in Fig. 6 and Fig. S8 of the ESI. From these diagrams it can be observed that, at low pH, the $[Cu_2H_i\mathbf{L}(A)]$ species are dominant and coexist with small amounts of $[Cu(ADP)]^{2-}$ (Fig. S8), $[Cu(ATP)]^{2-}$ and $[Cu(PPi)]^{2-}$ (Fig. 6). Then, around physiological pH, the $[Cu_2\mathbf{L}H_{-1}(A)]$ species are dominant, in all cases, indicating that the dicopper(II) complexes do not dissociate in the presence of polyphosphate anions.

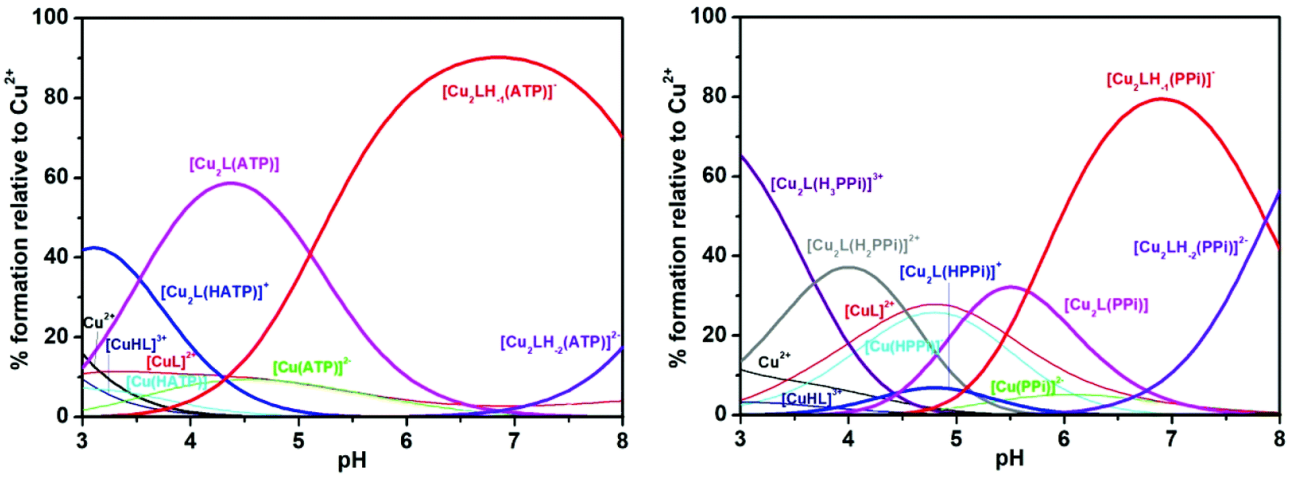

Fig. 6. Species distribution diagrams for the cascade species formed between the copper(II) complexes of **L** and ATP^{4-} (left) or $HPPi^{3-}$ (right) at 2 : 1 : 3 Cu^{2+}/**L**/A stoichiometry. $C_{Cu} = 2C_{\mathbf{L}} = 1/3\ C_A = 2.0 \times 10^{-3}$ M. A denotes the anion.

The association constants of the cascade species increase with the charge of the anion, the K_{eff} taking the highest values for ATP^{4-} and then for $HPPi^{3-}$ (Fig. 7), indicating the significant contribution of the electrostatic interactions. At low pH, aep^{2-} exhibits the highest K_{eff} value of about 5 at pH = 3.0, due to the reaction of $[CuHaep]^+$ with $[Cu\mathbf{L}]^{2+}$ complexes to form the $[Cu_2H\mathbf{L}(aep)]^{3+}$ species. The $[Cu_2\mathbf{L}H_{-1}A]$ cascade complex is the dominant species observed from pH ~ 6.0 to ~8 for all the anions, except for $Haep^-$, for which the predominant species in this pH range is $[Cu_2\mathbf{L}aep]^{2+}$ (see also the distribution species diagrams of Fig. S8 in the ESI).

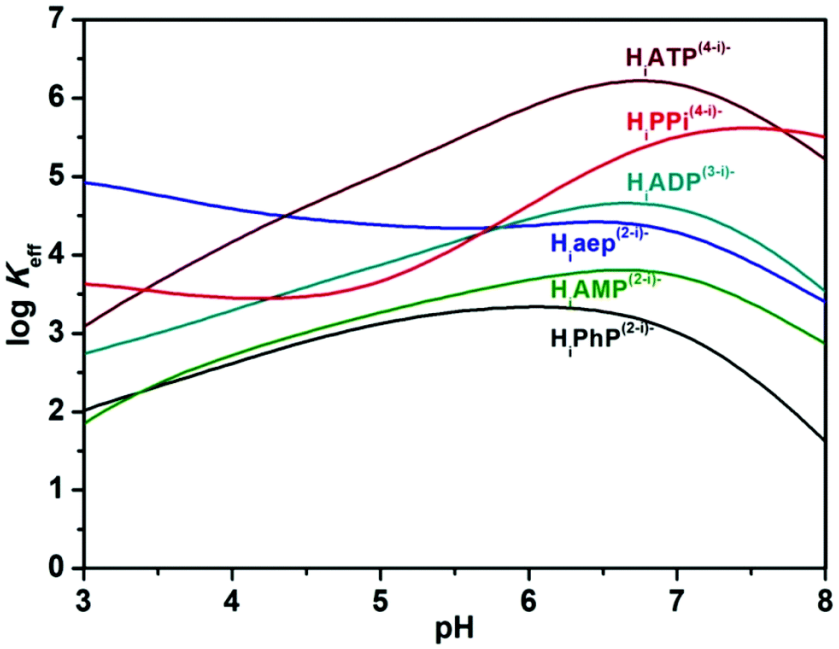

Fig. 7. Representation of the effective conditional constants as a function of pH for the cascade species studied. A is the anionic substrate; K_{eff} = ∑(total Cu bound to A)/∑(total A not bound to Cu) × ∑(total Cu not bound to A).[25]

The competition diagram plotted with the presence of all the anions under study shows that from pH about 4.5 to 7.8 ATP^{4-} is the anion bound to the receptor in higher amounts and then $HPPi^{3-}$ takes its place (Fig. 8). At pH 7.4, the copper(II) dinuclear squaramide-based receptor binds the anions following the trend: PhP^{2-} < AMP^{2-} < $Haep^{-}$ < ADP^{3-} < $HPPi^{3-}$ < ATP^{4-}. Comparable association constants were reported recently for different dpa-based receptors, which were found to be selective for $HPPi^{3-}$.[23] At physiologic pH and in the absence of $HPPi^{3-}$, ATP^{4-} is selectively taken by the dinuclear copper complex of **L**.

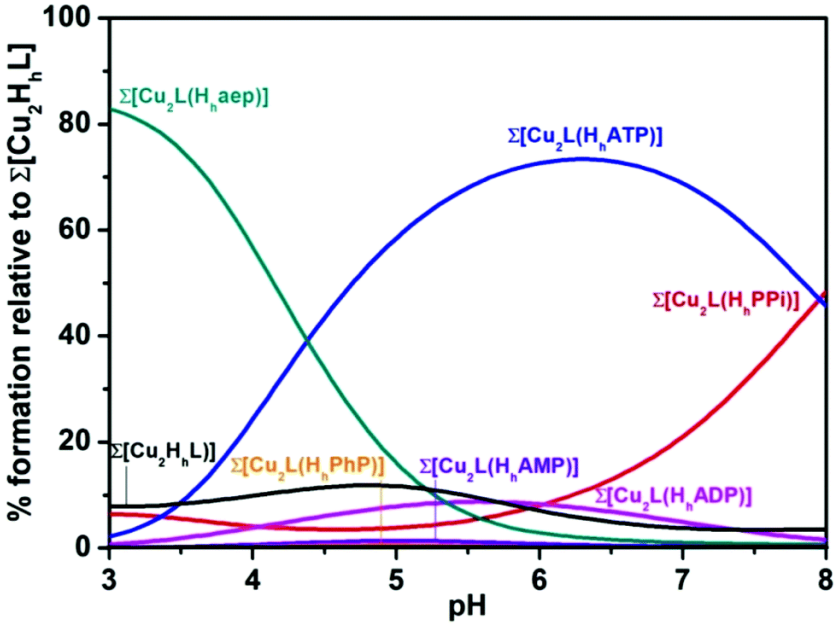

Fig. 8. Competition distribution diagram of the overall amounts of the supramolecular species formed between $[Cu_2H_h\mathbf{L}]^{4+h}$ and each anion. $C_{Cu} = 2C_L = 2C_A = 2.0 \times 10^{-3}$ M; L denotes the ligand and A the anion.

DFT calculations were also carried out to rationalize the observed anion affinity trend. The binding of PPi^{4-} was explored by considering different binding modes: A κ^2-PPi^{4-} chelate coordination to one of the copper(II) centres (Fig. S24a of the ESI),[23] a $\mu_2\kappa^4$-PPi^{4-} coordination involving the formation of two four-membered chelate rings (Fig. S24b of the ESI), and a $\mu_2\kappa^4$-PPi^{4-} coordination forming six-membered chelate rings (Fig. 5c). The corresponding free energy values indicate that the bridging coordination with formation of six-membered rings is more stable than the $\mu_2\kappa^4$-PPi^{4-} coordination leading to four-membered rings (+17.1 kJ mol^{-1}) and the κ^2-PPi^{4-} chelate coordination (+160.4 kJ mol^{-1}). Thus, these results strongly support the fact that the presence of the two metal centres provides a synergistic effect for the coordination of pyrophosphate. A $\mu_2\kappa^4$-PPi^{4-} coordination forming six-membered chelate rings was observed in the solid state for different complexes of PPi^{4-}.[24] The DFT calculations suggest that ATP^{4-} binds to the dinuclear complex through a similar $\mu_2\kappa^4$-PPi^{4-} coordination (Fig. 5c). Furthermore, the DFT structure presents hydrogen-bonding interactions involving the hydroxyl groups of the ribose unit and the oxygen atoms of the squaramide spacer. These results suggest that the selective recognition of ATP^{4-} occurs through a synergistic binding of the anion to the two metal centres reinforced by the presence of hydrogen bonds (Fig. 5d).

Conclusions

In the present work, a new unsymmetrical squaramide-based ligand bearing dipicolylamine (dpa) and ethylpiperazine units (**L**) was synthesized. This ligand is capable of forming stable dinuclear copper complexes upon deprotonation of the squaramidic nitrogen of the ethylpiperazine arm, with each copper centre likely having two water molecules to complete the coordination sphere, as supported by DFT calculations. The water molecules can be partially replaced by the O-donors of anions. Accordingly, the dicopper(II) complexes of **L**, $[Cu_2\mathbf{L}H_{-i}]^{4-i}$, were used as receptors for the uptake of some mono- and polyphosphate anions in aqueous solution. It was found that the receptor presents very high binding constants with ATP^{4-} and $HPPi^{3-}$. Additionally, the K_{eff} values indicated that, at physiological pH, the ATP^{4-} is selectively removed from an aqueous solution containing phenylphosphate ($PhPO_4^{2-}$), aminoethylphosphate ($Haep^-$), AMP^{2-} and ADP^{3-}, but $HPPi^{3-}$ strongly interferes. DFT calculations suggest that the PPi recognition is accomplished by $\mu_2\kappa^4$-PPi^{4-} coordination of the anion to the two metal ions, and the favoured recognition of ATP^{4-} occurs through a synergistic binding of the anion to the two metal centres reinforced by hydrogen-bonding interactions involving the hydroxyl groups of the ribose unit and the oxygen atoms of the squaramide spacer.

Experimental section

Materials and methods

All chemicals and solvents were purchased from commercial sources as reagent grade quality and used as received. The ^1H, $^{13}C\{^1H\}$ and $^{15}N\{^1H\}$ NMR spectra were recorded on a Bruker Avance II + 400 (^1H at 400.13 MHz and ^{13}C at 100.61 MHz) or a Bruker Avance II + 500 (^1H at 500.13, ^{13}C at 125.76 and $^{15}N\{^1H\}$ at 50.67 MHz) equipped with a 5 mm TCI C/N Prodigy Cryo probe spectrometer at a probe temperature of 298.2 K. Chemical shifts (δ) are given in parts per million relative to tetramethylsilane (TMS) used as the internal reference for ^1H NMR spectra in $CDCl_3$, and to 3-(trimethylsilyl)propionic-2,2,3,3-d_4 acid sodium salt (TSP-d_4) used as the internal reference for ^1H NMR spectra in D_2O. Assignments are based on peak integration and multiplicity and on 2D experiments (Fig. S9–S21 of the ESI). Microanalyses and electrospray mass spectra (ESI-MS) were carried out by the ITQB Analytical Services Unit.

Syntheses

Synthesis of 3-(bis(pyridin-2-ylmethyl)amino)-4-ethoxycyclobut-3-ene-1,2-dione, smdpa. Diethyl squarate (0.255 g, 1.5 mmol) was taken in diethyl ether (1 mL) and placed on a round bottom flask cooled by an ice bath. 2,2′-Dipicolylamine (0.598 g, 3.0 mmol) was also dissolved in diethyl ether (19 mL) and added dropwise to the round bottom flask. The mixture was stirred only while the addition was occurring. The mixture was left standing at r.t. under nitrogen for one week. The etheric solution was decanted and fine white crystalline needles grew in few minutes. The crystals were filtered, washed with diethyl ether (5 mL) and dried under vacuum (0.276 g, 57%). ^{1}H NMR (400 MHz, $CDCl_3$): δ 8.56 (2 H, t, H_{Py}), 7.69 (2 H, t, H_{Py}), 7.35 (1 H, d, H_{Py}), 7.24 (3 H, t, H_{Py}), 5.02 (2 H, s, CH_2–Py), 4.79 (2 H, s, CH_2–Py), 4.75 (2 H, q, CH_2–CH_3), 1.94 (3 H, br, NH–Py), 1.39 (3 H, t, CH_3) ppm. ^{13}C NMR (100 MHz, $CDCl_3$): δ 188.9, 183.2, 177.1 (C=O), 173.0 (C=N), 155.3, 155.2, 149.9, 149.4 (C=N_{Py}), 137.5, 137.1, 123.6, 123.3, 123.1, 122.5 (C_{Py}), 70.0 (–CH_2–), 54.6, 53.7 (CH_2–Py), 16.0 (–CH_3) ppm. Anal. calcd for $C_{18}H_{17}N_3O_3$: C, 66.9; H, 5.3; N, 13.0%. Found: C, 66.7; H, 5.2; N, 12.9%. ESI-MS (MeOH) *m*/*z*: 324.1 (100) [M + H^+] (Fig. S22).

Synthesis of 3-(bis(pyridin-2-ylmethyl)amino)-4-((2-(piperazin-1-yl)ethyl)amino)-cyclobut-3-ene-1,2-dione, L. The **smdpa** compound (0.253 g, 0.782 mmol) was taken in ethanol (35 mL) and placed on a round bottom flask. 2-(Piperazin-1-yl)ethan-1-amine (0.101 g, 0.782 mmol) was also dissolved in ethanol (10 mL) and added dropwise to **smdpa**. The mixture was stirred at r.t. under nitrogen for three days. The ethanolic solution was evaporated to dryness and the residue was taken in diethyl ether. The product was extracted to water (3 × 15 mL). KOH pellets were added to increase the pH to ~11 and the product was extracted with chloroform (3 × 15 mL) on its deprotonated form. The combined organic phases were dried with anhydrous Na_2SO_4, filtered, and evaporated to dryness under vacuum yielding a slightly yellow oil (0.295 g, 96%). ^{1}H NMR (400 MHz, D_2O/DCl): δ 8.69 (2 H, d, H_{Py}), 8.53 (2 H, t, H_{Py}), 8.01 (2 H, d, H_{Py}), 7.93 (2 H, t, H_{Py}), 5.25 (4 H, s, CH_2–Py), 3.98 (2 H, t, CH_2–CH_2), 3.63–3.56 (8H, br, CH_2-pip), 3.47 (2 H, t, CH_2–CH_2) ppm. ^{13}C NMR (100 MHz, $CDCl_3$): δ 184.1, 183.0 (C=O), 169.0, 168.4 (C=N), 155.5 (C=N_{Py}), 149.3, 137.5, 124.0, 123.3 (CH_{Py}), 59.1 (CH_2–CH_2), 54.9, 54.5 (CH_2–Py), 46.1 (CH_{2pip}), 41.0 (CH_2–CH_2) ppm. Anal. calcd for $C_{22}H_{26}N_6O_2$: C, 65.0; H, 6.5; N, 20.7%. Found: C, 65.1; H, 6.3; N, 21.0%. ESI-MS (MeOH) *m*/*z*: 407.2 (100) [M + H^+] (Fig. S23).

Single crystal X-ray diffraction

Crystals of **smdpa** suitable for X-ray diffraction determination were obtained as described above. X-ray diffraction data were collected with François Michaud (University of Brest) an X-Calibur-2 CCD 4-circle diffractometer (Oxford Diffraction), including a four-circle goniometer (KM4) and a two-dimensional CCD detector (SAPPHIRE 2). Three-dimensional X-ray diffraction data were collected on an X-Calibur-2 CCD 4-circle diffractometer (Oxford Diffraction). Data reduction, including interframe scaling, Lorentzian, polarization, empirical absorption, and detector sensitivity corrections, was carried out using programs that are part of CrysAlis software[26] (Oxford Diffraction). Complex scattering factors were taken from the program SHELX97[27] running under the WinGX program system.[28] The structure was solved by direct methods with SIR-97[29] and refined by full-matrix least-squares on F^2. All hydrogen atoms were included in calculated positions and refined in riding mode. Crystal data and details of the data collection and refinement are summarized in Table 4. The structure has been deposited in the Cambridge Structural Database as CCDC 1907210.

Table 4. Crystal data and refinement details of **smdpa**.

	smdpa
Formula	$C_{18}H_{17}N_3O_3$
MW	323.35
Crystal system	Monoclinic
Space group	$P2_1/n$
T/K	100(2)
a/Å	10.7368(6)
b/Å	10.5661(6)
c/Å	14.2037(8)
α/°	90
β/°	92.133(5)
γ/°	90
v/Å^3	1610.24(16)
F(000)	680.0
Z	4
λ, Å (MoK_α)	0.71073
D_{calc}/g cm^{-3}	1.334
μ/mm^{-1}	0.093
θ range/°	3.46 to 26.37
R_{int}	0.0798
Reflns collect.	10 126
Unique reflns	3290
GOF on F^2	1.024
R_1 [a]	0.0510
wR_2 (all data)[b]	0.1110
Largest diff peak and hole/e Å^{-3}	0.206 and −0.215

[a] $R_1 = \sum||F_o| - |F_c||/\sum|F_o|$. [b] $wR_2 = \{\sum[w(|F_o|^2 - |F_c|^2)^2]/\sum[w(F_o^4)]\}^{1/2}$.

Potentiometric measurements

The potentiometric system used was previously described.[30] Purified water from a Milli-Q demineralization system was used to prepare stock solutions of **L** prepared at *ca.* 2.00×10^{-3} M, and metal ion solutions prepared at 5.00×10^{-2} M from analytical grade nitrate salts standardized by titration with Na_2H_2edta.[31] Carbonate-free solutions of KOH were prepared from an ampoule diluted to make up 1 L of titrant, using freshly boiled water allowed to cool under nitrogen, standardized afterwards by application of Gran's method.[32] A 1.00×10^{-1} M standard solution of HNO_3 prepared also from an ampoule was used for backtitrations. The $[H^+]$ of the solutions was determined by measurement of the electromotive force of the cell, $E = E^{\circ\prime} + Q \log[H^+] + E_j$. The term pH is defined as $-\log[H^+]$. $E^{\circ\prime}$ and Q were determined by titrating a solution of known H-ion concentration at the same ionic strength in the acid pH region. The liquid-junction potential, E_j, was found to be negligible under the experimental conditions used. The value of $K_w = [H^+][OH^-]$ was found to be equal to $10^{-13.78}$ by titrating a solution of known H-ion concentration at the same ionic strength in the alkaline pH region, considering $E^{\circ\prime}$ and Q valid for the entire pH range. For the ligand determinations, a *ca.* 4.00×10^{-2} mmol solution was used in a total volume of *ca.* 30 mL, and for the copper(II) complexation studies and cascade species formed with anions a stabilized stock solution with *ca.* 2.0 equiv. of copper(II) was used. For the anions under study, measurements were carried out

with *ca.* 4.00 × 10^{-2} mmol of anions in a total volume of *ca.* 30 mL, in the absence and in the presence of *ca.* 1.0 equiv. of copper(II). In the case of PPi^{4-} and of aep^{2-} measurements were carried out with *ca.* 4.00 × 10^{-2} mmol of anions in a total volume of *ca.* 50 mL, in the absence and in the presence of *ca.* 1.0 equiv. of copper(II), to avoid the formation of precipitates. A backtitration was always performed at the end of each direct titration in order to check if equilibrium was attained throughout the full pH range. Each titration curve consisted of 40–100 points, depending on the system under study, in the 2.5–11.5 pH range, and a minimum of two replicate titrations were performed for each system.

Determination of thermodynamic equilibrium constants

The overall protonation constants of the ligand and of the anions under study, β^{H}_{i}, the overall stability constants of complexes formed with the ligand or with the anions, $\beta_{Cum}H_{h}\mathbf{L}$ and $\beta_{Cum}H_{h}A$, the overall association constants of the anions with protonated forms of the ligand, β_{HhLA}, and the overall association constants of the copper(II) complexes with the anions, $\beta_{Cum}H_{h}\mathbf{L}A$, were calculated by fitting the potentiometric data of the titrations with the HYPERQUAD program,[33] and by fitting the ^{1}H NMR titration data with the HYPNMR program.[34] At least two titration curves for each system were fitted together. The initial computations were obtained in the form of overall constants, $\beta_{Hh\mathbf{L}} = [H_h\mathbf{L}]/[H]^h[\mathbf{L}]$, $\beta_{Cum}H_{h\mathbf{L}} = [Cu_mH_h\mathbf{L}]/[Cu]^m[H]^h[\mathbf{L}]$, $\beta_{Cum}H_{h-1}\mathbf{L} = \beta_{Cum}\mathbf{L}(OH) \times K_w$, and $\beta_{Cum}H_{h\mathbf{L}A} = [Cu_mH_h\mathbf{L}A]/[Cu]^m[H]^h[\mathbf{L}][A]$. In all cases A = studied anions. The errors quoted are standard deviations of the overall constants given directly by the program for the input data, which include all of the experimental points of all titration curves. The HYSS program[25] was used to calculate the concentration of equilibrium species from the calculated constants from which distribution diagrams were plotted. The species considered in a particular model were those that could be justified according to the principles of coordination and supramolecular chemistry.

NMR measurements

^{1}H, ^{13}C NMR, HSQC, HMBC and NOESY spectra were recorded at 298.2 K on a Bruker AVANCE III 500 spectrometer (Bruker, Rheinstetten, Germany) operating at a proton central frequency of 500.13 MHz equipped with a triple resonance inverse CryoProbe Prodigy (TCI) with pulsed field gradients in all titrations. When D_2O was used as the solvent, ^{1}H NMR spectra were acquired using a pre-saturation of the residual water signal and chemical shifts are relative to 3-(trimethylsilyl)propionic-2,2,3,3-d_4 acid sodium salt (TSP-d_4). In $CDCl_3$, chemical shifts were referenced to tetramethylsilane (TMS). ^{13}C NMR spectra were typically acquired with proton decoupling during the acquisition time using the WALTZ-64 sequence.[35] Two dimensional spectra were acquired using standard Bruker NMR pulse sequences. NMR spectra were processed with MestReNova 9.0 (Mestrelab Research, Santiago de Compostela, Spain). Solutions of **L** were prepared at a concentration of 1.5 × 10^{-2} M in H_2O–D_2O, in D_2O and in $CDCl_3$. Titrations were performed directly in the NMR tube and the observed pH (pH*), monitored with a pH/ISE meter from a ThermoScientific model Orion Star A214 fitted with a combined microelectrode from a Hamilton model Sprintrode P/N238197/04. When H_2O/D_2O or D_2O was used the pH (or pD) was changed by addition of DCl stock solutions of 0.1, 0.5 or 1.0 M or NaOD (CO_2 free and freshly prepared) solutions of 1.0 and 0.1 M. The microelectrode was calibrated with commercial buffers in aqueous solution (pH of 12.00, 8.00, and 4.00). The final pD was calculated according to the equation pD = pH* + (0.40 ± 0.02),[12] where pH* corresponds to the pH readings from the pH meter.

UV-vis measurements

All spectra were obtained at 298 K in buffered aqueous solution ([MOPS] = 2.5 × 10^{-2} M, pH = 7.4) on a PerkinElmer UV-vis spectrophotometer Lambda 650. The solutions were prepared in vials for the batch acquisition using the mother solutions of **L** (7.23 × 10^{-3} M) and $Cu(NO_3)_2$ (4.98 × 10^{-2} M) in a total volume of 1.2 mL. Each vial contained increments of about 0.15 equiv. of copper(II) yielding a concentration in the vis region of 2.89 × 10^{-3} M, and in the UV region of 2.89 × 10^{-5} M.

DFT calculations

All DFT calculations were carried out using the Gaussian 09 package (Revision E.01).[36] The hybrid *meta*-GGA approximation with the TPSSh[37] exchange–correlation functional was used throughout, in combination with Ahlrich's valence triple-ξ basis set with polarization functions (TZVP).[38] Solvent effects (water) were considered with the integral equation formalism variant of the polarizable continuum model (IEFPCM).[39] The stationary points obtained after geometry optimization were characterized by frequency analysis using the harmonic oscillator approximation.

Conflicts of interest

There are no conflicts to declare.

Acknowledgements

This work was partially supported by Project LISBOA-01-0145-FEDER-007660 (Microbiologia Molecular, Estrutural e Celular) funded by FEDER funds through COMPETE2020 – Programa Operacional Competitividade e Internacionalização (POCI) and by national funds through FCT. The NMR data were acquired at CERMAX, ITQB-NOVA, Oeiras, Portugal with equipment funded by FCT, project AAC 01/SAICT/2016. C. V. Esteves thanks FCT for the PhD fellowship SFRH/BD/89501/2012 and Project LISBOA-01-0145-FEDER-007660 for a last fellowship.

References

01 (*a*) Q. He, P. Tu and J. L. Sessler, *Chem*, 2018, **4**, 46–93; (*b*) P. A. Gale, E. N. W. Howe, X. Wu and M. J. Spooner, *Coord. Chem. Rev.*, 2018, **375**, 333–372; (*c*) J. Zhao, D. Yang, X.-J. Yang and B. Wu, *Coord. Chem. Rev.*, 2019, **378**, 415–444; (*d*) N. Busschaert, C. Caltagirone, W. V. Rossom and P. A. Gale, *Chem. Rev.*, 2015, **115**, 8038–8155.

02 R. Prohens, S. Tomàs, J. Morey, P. M. Deyà, P. Ballester and A. Costa, *Tetrahedron Lett.*, 1998, **39**, 1063–1066.

03 (*a*) R. Prohens, G. Martorell, P. Ballester and A. Costa, *Chem. Commun.*, 2001, 1456–1457; (*b*) R. Prohens, M. C. Rotger, M. N. Piña, P. M. Deyà, J. Morey, P. Ballester and A. Costa, *Tetrahedron Lett.*, 2001, **42**, 4933–4936; (*c*) A. Frontera, J. Morey, A. Oliver, M. N. Piña, D. Quiñonero, A. Costa, P. Ballester and P. M. Deyà, *J. Org. Chem.*, 2006, **71**, 7185–7195; (*d*) M. N. Piña, C. Rotger, B. Soberats, P. Ballester, P. M. Deyà and A. Costa, *Chem. Commun.*, 2007, 963–965; (*e*) M. N. Piña, B. Soberats, C. Rotger, P. Ballester, P. M. Deyà and A. Costa, *New J. Chem.*, 2008, **32**, 1919–1923; (*f*) V. Amendola, G. Bergamaschi, M. Boiocchi, L. Fabbrizzi and M. Milani, *Chem. – Eur. J.*, 2010, **16**, 4368–4380; (*g*) A. Rostami, A. Colin, X. Y. Li, M. G. Chudzinski, A. J. Lough and M. S. Taylor, *J. Org. Chem.*, 2010, **75**, 3983–3992; (*h*) B. Soberats, L. Martínez, E. Sanna, A. Sampedro, M. C. Rotger and A. Costa, *Chem. – Eur. J.*, 2012, **18**, 7533–7542; (*i*) N. Busschaert, I. L. Kirby, S. Young, S. J. Coles, P. N. Horton, M. E. Light and P. A. Gale, *Angew. Chem., Int. Ed.*, 2012, **51**, 4426–4430; (*j*) C. Jin, M. Zhang, C. Deng, Y. Guan, J. Gong, D. Zhu, Y. Pan, J. Jiang and L. Wang, *Tetrahedron Lett.*, 2013, **54**, 796–801; (*k*) C. Jin, M. Zhang, L. Wu, Y. Guan, Y. Pan, J. Jiang, C. Lin and L. Wang, *Chem. Commun.*, 2013, **49**, 2025–2027; (*l*) R. B. P. Elmes, P. Turner and K. A. Jolliffe, *Org. Lett.*, 2013, **15**, 5638–5641; (*m*) L.-Q. Deng, Y.-M. Lu, C.-Q. Zhou, J.-X. Chen, B. Wang and W.-H.

Chen, *Bioorg. Med. Chem. Lett.*, 2014, **24**, 2859–2862; (*n*) S. J. Edwards, H. Valkenier, N. Busschaert, P. A. Gale and A. P. Davis, *Angew. Chem., Int. Ed.*, 2015, **54**, 4592–4596; (*o*) X. Wu, N. Busschaert, N. J. Wells, Y.-B. Jiang and P. A. Gale, *J. Am. Chem. Soc.*, 2015, **137**, 1476–1484; (*p*) L. Qin, A. Hartley, P. Turner, R. B. Elmes and K. A. Jolliffe, *Chem. Sci.*, 2016, **7**, 4563–4572; (*q*) Y. Li, G.-H. Yang, Y.-Y. Shen, X.-S. Xue, X. Li and J.-P. Cheng, *J. Org. Chem.*, 2017, **82**, 8662–8667; (*r*) X. Bao, X. Wu, S. N. Berry, E. N. W. Howe, Y.-T. Chang and P. A. Gale, *Chem. Commun.*, 2018, **54**, 1363–1366.

04 (*a*) R. I. Storer, C. Aciro and L. H. Jones, *Chem. Soc. Rev.*, 2011, **40**, 2330–2346; (*b*) F. R. Wurm and H.-A. Klok, *Chem. Soc. Rev.*, 2013, **42**, 8220–8236; (*c*) X.-J. Cai, Z. Li and W.-H. Chen, *Mini-Rev. Org. Chem.*, 2018, **15**, 148–156.

05 E. Sanna, L. Martínez, C. Rotger, S. Blasco, G. González, E. García-España and A. Costa, *Org. Lett.*, 2010, **12**, 3840–3843.

06 G. Ambrosi, M. Formica, V. Fusi, L. Giorgi, A. Guerri, M. Micheloni, P. Paoli, R. Pontellini and P. Rossi, *Chem. – Eur. J.*, 2007, **13**, 702–712.

07 A. H. Smith, *Synthesis*, 1980, 961–994.

08 (*a*) E. W. Neuse and B. R. Green, *J. Org. Chem.*, 1974, **39**, 3881–3887; (*b*) A. Mukkanti and M. Periasamy, *ARKIVOC*, 2005, **xi**, 48–77.

09 M. C. Rotger, M. N. Piña, A. Frontera, G. Martorell, P. Ballester, P. M. Deyà and A. Costa, *J. Org. Chem.*, 2004, **69**, 2302–2308.

10 F. Khalili, A. Henni and A. L. L. East, *J. Chem. Eng. Data*, 2009, **54**, 2914–2917.

11 G. Anderegg, E. Hubmann, N. G. Podder and F. Wenk, *Helv. Chim. Acta*, 1977, **60**, 123–140.

12 R. Delgado, J. J. R. Fraústo da Silva, M. T. S. Amorim, M. F. Cabral, S. Chaves and J. Costa, *Anal. Chim. Acta*, 1991, **245**, 271–282.

13 A. KrÈ©żel and W. Bal, *J. Inorg. Biochem.*, 2004, **98**, 161–166.

14 G. Popa and V. Magearu, *Rev. Roum. Chim.*, 1969, **14**, 1387.

15 I. Lukes, K. Bazakas, P. Hermann and P. Vojtisek, *J. Chem. Soc., Dalton Trans.*, 1992, 939–944 .

16 S. Kumari, A. K. Mahato, A. Maurya, V. K. Singh, N. Kesharwani, P. Kachhap, I. O. Koshevoy and C. Haldar, *New J. Chem.*, 2017, **41**, 13625–13646.

17 (*a*) N. Niklas, F. W. Heinemann, F. Hampel, T. Clark and R. Alsfasser, *Inorg. Chem.*, 2004, **43**, 4663–4673; (*b*) N. Niklas, F. Hampel, G. Liehr, A. Zahl and R. Alsfasser, *Chem. – Eur. J.*, 2001, **7**, 5135–5142.

18 S. Sopeña, E. Martin, E. C. Escudero-Adan and A. W. Kleij, *ACS Catal.*, 2017, **7**, 3532–3539.

19 A. Subasinghe, I. C. Perera, S. Pakhomova and T. Perera, *Bioinorg. Chem. Appl.*, 2016, 2675937, DOI:10.1155/2016/2675937, 10 pages.

20 (*a*) I. Carreira-Barral, T. Rodriguez-Blas, C. Platas-Iglesias, A. de Blas and D. Esteban-Gómez, *Inorg. Chem.*, 2014, **53**, 2554–2568; (*b*) I. Carreira-Barral, M. Mato-Iglesias, A. de Blas, C. Platas-Iglesias, P. A. Tasker and D. Esteban-Gómez, *Dalton Trans.*, 2017, **46**, 3192–3206.

21 (*a*) H. Keypour, M. Mahmoudabadi, A. Shooshtari, M. Bayat, R. Karamian, M. Asadbegy and R. W. Gable, *Inorg. Chim. Acta*, 2018, **478**, 176–186; (*b*) M. G. Amiri and H. Golchoubian, *J. Mol. Struct.*, 2018, **1165**, 196–205.

22 C. V. Esteves, D. Esteban-Gómez, C. Platas-Iglesias, R. Tripier and R. Delgado, *Inorg. Chem.*, 2018, **57**, 6466–6478.

23 I. Carreira-Barral, I. Fernandez-Perez, M. Mato-Iglesias, A. de Blas, C. Platas-Iglesias and D. Esteban-Gomez, *Molecules*, 2018, **23**, 479.

24 (*a*) R. P. Sartoris, O. R. Nascimento, R. C. Santana, M. Perec, R. F. Baggio and R. Calvo, *Dalton Trans.*, 2015, **44**, 4732–4743; (*b*) J. H. Lee, J. Park, M. S. Lah, J. Chin and J.-I. Hong, *Org. Lett.*, 2007, **9**, 3729–3731.

25 L. Alderighi, P. Gans, A. Ienco, D. Peters, A. Sabatini and A. Vacca, *Coord. Chem. Rev.*, 1999, **184**, 311–318.

26 *CrysAlis software system, version 1.171.28 cycle4 beta*, Oxford Diffraction Ltd., Abingdon, U.K., 2005.

27 G. M. A. Sheldrick, Short History of SHELX, *Acta Crystallogr., Sect. A: Found. Crystallogr.*, 2008, **64**, 112–122.

28 L. J. Farrugia, WinGX MS-Windows System of Programs for Solving, Refining and Analysing Single Crystal X-ray Diffraction Data for small Molecules, *J. Appl. Crystallogr.*, 1999, **32**, 837–838.

29 A. Altomare, M. C. Burla, M. Camalli, G. L. Cascarano, C. Giacovazzo, A. Guagliardi, A. G. G. Moliterni, G. Polidori and R. Spagna, SIR97: A New Tool for Crystal Structure Determination and Refinement, *J. Appl. Crystallogr.*, 1999, **32**, 115–119.

30 C. V. Esteves, P. Mateus, V. André, N. A. G. Bandeira, M. J. Calhorda, L. P. Ferreira and R. Delgado, *Inorg. Chem.*, 2016, **55**, 7051–7060.

31 G. Schwarzenbach and W. Flaschka, *Complexometric Titrations*, Methuen & Co, London, 1969.

32 F. J. C. Rossotti and H. Rossotti, *J. Chem. Educ.*, 1965, **42**, 375–378.

33 P. Gans, A. Sabatini and A. Vacca, *Talanta*, 1996, **43**, 1739–1753.

34 C. Frassineti, S. Ghelli, P. Gans, A. Sabatini, M. S. Moruzzi and A. Vacca, *Anal. Biochem.*, 1995, **231**, 374–382.

35 A. J. Shaka, P. B. Barker and R. Freeman, *J. Magn. Reson.*, 1985, **64**, 547–552.

36 M. J. Frisch, G. W. Trucks, H. B. Schlegel, G. E. Scuseria, M. A. Robb, J. R. Cheeseman, G. Scalmani, V. Barone, B. Mennucci, G. A. Petersson, H. Nakatsuji, M. Caricato, X. Li, H. P. Hratchian, A. F. Izmaylov, J. Bloino, G. Zheng, J. L. Sonnenberg, M. Hada, M. Ehara, K. Toyota, R. Fukuda, J. Hasegawa, M. Ishida, T. Nakajima, Y. Honda, O. Kitao, H. Nakai, T. Vreven, J. A. Montgomery Jr., J. E. Peralta, F. Ogliaro, M. Bearpark, J. J. Heyd, E. Brothers, K. N. Kudin, V. N. Staroverov, R. Kobayashi, J. Normand, K. Raghavachari, A. Rendell, J. C. Burant, S. S. Iyengar, J. Tomasi, M. Cossi, N. Rega, N. J. Millam, M. Klene, J. E. Knox, J. B. Cross, V. Bakken, C. Adamo, J. Jaramillo, R. Gomperts, R. E. Stratmann, O. Yazyev, A. J. Austin, R. Cammi, C. Pomelli, J. W. Ochterski, R. L. Martin, K. Morokuma, V. G. Zakrzewski, G. A. Voth, P. Salvador, J. J. Dannenberg, S. Dapprich, A.

D. Daniels, Ö. Farkas, J. B. Foresman, J. V. Ortiz, J. Cioslowski and D. J. Fox, *Gaussian 09, Revision E.01*, Gaussian, Inc., Wallingford CT, 2009.

37 J. M. Tao, J. P. Perdew, V. N. Staroverov and G. E. Scuseria, *Phys. Rev. Lett.*, 2003, **91**, 146401.

38 A. Schaefer, C. Huber and R. Ahlrichs, *J. Chem. Phys.*, 1994, **100**, 5829–5835.

39 J. Tomasi, B. Mennucci and R. Cammi, *Chem. Rev.*, 2005, **105**, 2999–3093.

[i] Electronic supplementary information (ESI) available: Tables of the overall and stepwise protonation constants of 2-aminoethylphosphonic acid, stability constants of the copper(ii) complexes of the anions, overall association constants of the anions with protonated forms of **L**, and overall association constants of the copper(ii) complexes of **L** with the anions; crystal structure of **smdpa**; ^{1}H and ^{13}C NMR titration of **L** in D_2O; ^{1}H–^{15}N and ^{1}H–^{13}C HSQC spectra of **L** in $CDCl_3$; ^{1}H NMR spectra of **L** in presence of copper(ii) in $CDCl_3$, DMSO-d_6, and in H_2O/D_2O 9 : 1 v/v; titration in vis region of **L** with copper(ii); species distribution diagrams for the cascade complexes; ^{1}H, ^{13}C NMR, COSY and HMQC spectra of **smdpa** in $CDCl_3$; ^{1}H NMR and COSY spectra of **L** in D_2O/DCl; ^{1}H, ^{13}C NMR and HSQC spectra of **L** in D_2O; ^{1}H NMR, ^{13}C APT, HMBC and NOESY of **L** in $CDCl_3$; ESI mass spectra of smdpa and **L**; structures of the $[Cu_2\mathbf{L}H_{-1}(PPi)(H_2O)_2]^-$ and $[Cu_2\mathbf{L}H_{-1}(\mu_2\kappa^4\text{-PPi})]^-$ complexes obtained with DFT calculations; and the tables with the optimized Cartesian coordinates (Å) obtained for $[Cu\mathbf{L}(H_2O)_2]^{2+}$, $[Cu_2\mathbf{L}H_{-1}(H_2O)_4]^{3+}$, $[Cu_2\mathbf{L}H_{-1}(\kappa^2\text{-PPi})(H_2O)_2]^-$, $[Cu_2\mathbf{L}H_{-1}(\mu_2\kappa^4\text{-PPi})]^-$, and $[Cu_2(\mathbf{L}H_{-1})ATP]^-$. CCDC 1907210. For ESI and crystallographic data in CIF or other electronic format see DOI: 10.1039/c9dt01434a .